 DOI:10.30420/566414095

Adaptive Parametric Impedance Model Order Reduction Method for Grid-tied Renewable Energy Dominated Microgrid

Xun Jiang[1], Meiqin Mao[1], Bao Xie[1], Liuchen Chang[2], Haijiao Wang[3]

[1] Research Center for Photovoltaic System Engineering of Ministry of Education, Hefei University of Technology, China, China.

[2] University of New Brunswick, Canada.

[3] State Key Laboratory of Operation and Control of Renewable Energy & Storage Systems (China Electric Power Research Institute), China.

Corresponding author: Meiqin Mao, mmqmail@163.com

Speaker: Xun Jiang, jaysonxun@163.com

Abstract

The high-precision reduced order impedance model can significantly reduce the computation burden in the small-signal oscillatory instability detection process of grid-tied renewable energy dominated microgrids (REMGs). However, due to improper interpolation strategies, the existing model order reduction method cannot build the high-precision parametric reduced order impedance model (PROIM) for REMG. To fill these gaps, this paper proposes the adaptive parametric model order reduction method to build a high-precision PROIM for REMGs. In this method, the adaptive optimization of system parameters and frequency interpolation points is achieved by introducing the evaluation indexes including convergence error, cumulative error, and projection matrix rank. The error performance of the obtained PROIM by the proposed method and its efficiency in actual oscillatory stability analysis are validated by a small-scale REMG with 4 different converter-based renewable generators (CREGs) and a real-time simulation model using a large-scale REMG of 4.2 MW with 18 different CREGs.

1 Introduction

Along with the prevalence of renewable energy systems (RESs) in new paradigm power systems, an individual renewable energy dominated microgrid (REMG) is incapable to well organize large-scale RESs, more and more distributed REMGs are being meshed together as a microgrid cluster to feed more RESs efficiently and reliably into the power system [1].

However, the small-signal stability analysis (SSSA) of such REMG-dominated power systems faces huge computational challenges because of the extremely high order of the full-order model of the investigated power systems. Therefore, it is crucial to create a high-precision reduced-order model of each REMG which can be provided to the power system planners and operators as a tool for SSSA with a low computational burden [2].

The impedance model-based SSSA method can effectively deal with the oscillatory instability problems of grid-tied converter-based renewable energy generators (CREGs). Due to its universal applicability, intuitive stability criteria, and scalability for large systems, the impedance model-based SSSA method has been extended to the SSSA of REMGs [3]. In the current literature, the methods for the reduced-order impedance models (IMs) of REMGs can be divided into two categories: 1) Data-based methods; and 2) Full-order model-based methods. In the data-based methods, the frequency response data of REMGs must first be obtained by perturbing the operating REMGs with some proper signals, and then the reduced-order IMs are built by the vector fitting method [4]. The full-order IMs of REMGs do not need to be built in advance and the so-called grey-box modelling can be achieved by the data-based methods. However, it is not easy to obtain the frequency response data in actual REMGs [5], which hinders the development of the data-based method.

Therefore, at the current stage, the full-order model-based method is still the primary method to build the reduced-order IMs. In [6], the full-order IM of a practical wind farm is simplified to an RLC equivalent circuit around the oscillation frequency. This approach accurately assesses the risk of sub-synchronous resonance in practical wind farms and represents the first effort in recent years to reduce the computational burden of SSSA by simplifying the full-order IMs. However, the RLC equivalent circuit built by this method is only valid around the oscillation frequency. To date, the reduced-order IMs of wind farms in wide frequency bands are built by different model order reduction technologies, such as the balanced truncation method, without considering the parameter preserving [7].

In practice, the impedance characteristics of REMGs are influenced not only by the pre-set controller parameters of each CREG but also by the different system

ISBN 978-3-8007-6414-3

operation points of each CREG. The nonparametric reduced-order IMs only can be consistent with the original full-order IMs under specific parameter combinations, and they have great limitations in the SSSA of grid-tied REMG. In view of the above, it is critical to build the parametric reduced-order IMs (PROIMs) of REMGs which are precise enough to characterize system features for various system parameter values.

To date, the Krylov subspace-based parametric model order reduction (KS-PMOR) method has been presented to build the parametric reduced-order model for the large-scale circuit design of operational amplifiers [8]. In the KS-PMOR method, the accuracy of the obtained reduced-order model strongly depends on the adopted interpolation strategies [9]. However, as far as the authors know, there are no such general interpolation strategies available for the application of the KS-PMOR method in different fields. The general interpolation optimizing method needs to be carefully investigated before it is applied to build the precise PROIMs of REMGs.

To fill this gap, this paper originally proposes an adaptive parametric impedance model order reduction (AP-IMOR) method to build the high-precision PROIMs of the REMGs. The proposed method is evaluated based on a small-scale MCFSs with 4 different CREGs and a real-time simulation model for large-scale MCFS with 18 different CREGs.

2 Full-Order Impedance Model of the Investigated REMG

In the power system with clusters of REMGs, as shown in Fig. 1, various distributed REMGs incorporating numerous CREGs are tied to the grid in a regional area. For the investigated grid-tied REMG, N CREGs are parallelly connected to the same common bus via feeders. The DC-side power supply of each CREG can be provided by different forms of renewable energy generators, such as wind generators, photovoltaic generators, energy storage systems, and even grid-connected electrical vehicles, and its output power is controlled by a grid-following controller. L_g, L_m, R_d, and C denote the grid-side inductance, converter-side inductance, damping resistance, and filter capacitance of the CREG output filter, respectively. $Z_{line}=R_{line}+j\omega L_{line}$ is the equivalent impedance of the output feeder line of each CREG in the REMG. The small signal model of a single CREG with varying parameters λ can be expressed in (1).

$$\begin{cases} \dot{\boldsymbol{x}}_{dq} = \boldsymbol{A}_{C,dq}(\lambda)\boldsymbol{x}_{dq} + \boldsymbol{B}_{C,dq}(\lambda)\boldsymbol{u}_{dq} \\ \boldsymbol{y}_{dq} = \boldsymbol{C}_{C,dq}(\lambda)\boldsymbol{x}_{dq} \end{cases} \tag{1}$$

Based on the small signal model of a single CREG, the full-order small-signal model of REMG containing N CREGs with different parameters can be represented in the form of state-space equations, shown in (2) [10].

$$\begin{cases} \begin{pmatrix} \dot{\boldsymbol{x}}_1 \\ \vdots \\ \dot{\boldsymbol{x}}_i \end{pmatrix} = \begin{pmatrix} \boldsymbol{A}_{GFI,1} & 0 & 0 \\ 0 & \ddots & 0 \\ 0 & 0 & \boldsymbol{A}_{GFI,i} \end{pmatrix} \begin{pmatrix} \boldsymbol{x}_1 \\ \vdots \\ \boldsymbol{x}_i \end{pmatrix} + \begin{pmatrix} \boldsymbol{B}_{GFI,1} \\ \vdots \\ \boldsymbol{B}_{GFI,i} \end{pmatrix} \begin{pmatrix} \boldsymbol{u}_1 \\ \vdots \\ \boldsymbol{u}_i \end{pmatrix} \\ y = \begin{pmatrix} \boldsymbol{C}_{GFI,1} & \cdots & \boldsymbol{C}_{GFI,N} \end{pmatrix} \begin{pmatrix} \boldsymbol{x}_1 & \cdots & \boldsymbol{x}_i \end{pmatrix}^T \end{cases} \tag{2}$$

where, $\boldsymbol{A}_{GFI,i}$, $\boldsymbol{B}_{GFI,i}$, and $\boldsymbol{C}_{GFI,i}$ are the state matrix, input matrix, and output matrix of each CREG, respectively.

According to (2), the full-order IM Z_{MCFS} of REMG in transfer function form can be expressed as in (3).

$$Z_{MCFS}(s) = 1/(\boldsymbol{C}_{MCFS}(s\boldsymbol{I} - \boldsymbol{A}_{MCFS})^{-1}\boldsymbol{B}_{MCFS}) \tag{3}$$

where, $\boldsymbol{A}_{MCFS}=\mathrm{diag}(\boldsymbol{A}_{GFI,1}, \boldsymbol{A}_{GFI,2}, \ldots, \boldsymbol{A}_{GFI,i})$, $\boldsymbol{B}_{MCFS}=[\boldsymbol{B}_{GFI,1}, \boldsymbol{B}_{GFI,2}, \ldots, \boldsymbol{B}_{GFI,i}]^T$, $\boldsymbol{C}_{MCFS}=[\boldsymbol{C}_{GFI,1}, \boldsymbol{C}_{GFI,2}, \ldots, \boldsymbol{C}_{GFI,i}]$, $\boldsymbol{I}$ represents the identity matrix.

For the REMG including N parallel CREGs with identical parameters and operation setpoints, the IM of the REMG can be built by directly scaling the original full-

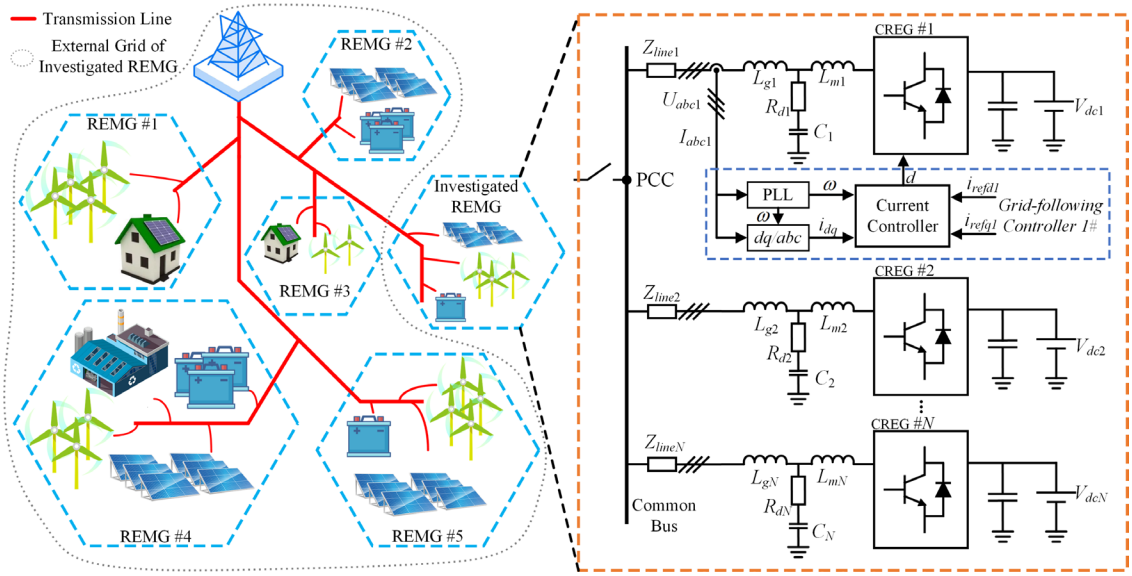

Fig. 1. Topology of power system with clusters of REMGs.

order small-signal model of individual CREGs. However, a typical REMG consists of a large number of CREGs with variable types and parameters. Its corresponding state equation (2) has an extremely high order and the IM of the REMG cannot be obtained by simply scaling the original full-order small signal model of the individual CREGs. As a result, the SSSA of power systems based on the full-order model of the REMG faces a huge computational burden.

3 Proposed Adaptive Parametric Impedance Model Order Reduction Method

3.1 Traditional KS-PMOR method

The full-order model of the typical REMG with varying parameters can be expressed as in (4).

$$\begin{cases} \boldsymbol{E}(p)\dot{x} = \boldsymbol{A}(p)\boldsymbol{x} + \boldsymbol{B}(p)u \\ y = \boldsymbol{C}(p)\boldsymbol{x} \end{cases} \tag{4}$$

where, $\boldsymbol{E}(p) \in \mathbb{R}^{n\times n}$, $\boldsymbol{A}(p) \in \mathbb{R}^{n\times n}$, $\boldsymbol{B}(p) \in \mathbb{R}^{n\times m}$, $\boldsymbol{C}(p) \in \mathbb{R}^{1\times n}$, $\boldsymbol{u} \in \mathbb{R}^{m\times 1}$, p is the varying parameter, $p \in \mathbb{S}$, $\mathbb{S}$ denoting the parameter space.

In the traditional KS-PMOR methods, the full-order model with varying parameters in (4) is projected to a low-dimensional state space by the projection matrix $\boldsymbol{T}_p \in \mathbb{C}^{r\times n}$ ($r \ll n$), as shown in (5), and the projection matrix $\boldsymbol{T}_p$ plays a key role in obtaining a high-precision parametric reduced order model.

$$\begin{cases} \boldsymbol{E}_r(p)\dot{x}_r = \boldsymbol{A}_r(p)\boldsymbol{x}_r + \boldsymbol{B}_r(p)u \\ y = \boldsymbol{C}_r(p)\boldsymbol{x}_r \end{cases} \tag{5}$$

where, $\boldsymbol{E}_r(p)=\boldsymbol{T}_p\boldsymbol{E}(p)\boldsymbol{T}_p^T$, $\boldsymbol{E}_r(p) \in \mathbb{C}^{r\times r}$, $\boldsymbol{A}_r(p)=\boldsymbol{T}_p\boldsymbol{A}(p)\boldsymbol{T}_p^T$, $\boldsymbol{A}_r(p) \in \mathbb{C}^{r\times r}$, $\boldsymbol{B}_r(p)=\boldsymbol{T}_p\boldsymbol{B}(p)$, $\boldsymbol{B}_r(p) \in \mathbb{C}^{r\times m}$, $\boldsymbol{C}_r(p)=\boldsymbol{C}(p)\boldsymbol{T}_p^T$, $\boldsymbol{C}_r(\boldsymbol{p}(t)) \in \mathbb{C}^{1\times r}$, $\boldsymbol{x}_r=\boldsymbol{T}_p\boldsymbol{x}$.

The state vectors $\boldsymbol{X}(s_i)$ in the frequency domain can be derived at several frequency interpolation points in the reduced-order frequency band Ω, and the obtained $\boldsymbol{X}(s_i)$ should satisfy the equation (6), which is derived from (4) by Laplace transform [8].

$$(s_i\boldsymbol{E}(p) - \boldsymbol{A}(p))\boldsymbol{X}(s_i) = \boldsymbol{B}(p) \tag{6}$$

where s_i represents the frequency interpolation points.

Then, the projection matrix $\boldsymbol{T}_p$ can be spanned by the $\boldsymbol{X}(s_i)$ at each frequency interpolation point, as in (7).

$$\boldsymbol{T}_\mathrm{p} \supseteq \mathrm{span}\{\boldsymbol{X}(s_1), \boldsymbol{X}(s_2), \cdots, \boldsymbol{X}(s_\mathrm{i})\} \tag{7}$$

According to the above discussions, the challenge in deriving $\boldsymbol{T}_p$ is actually a problem of solving $\boldsymbol{X}(s_i)$ precisely at appropriate frequency interpolation points. However, there is no explicit solution to $\boldsymbol{X}(s_i)$ satisfying all parameter values in $\mathbb{S}$. Here, the solution of $\boldsymbol{X}(s_i)$ satisfying equation (6) within the whole $\mathbb{S}$ is transferred to the optimization problem in (8).

$$\begin{cases} \min\limits_{\boldsymbol{X}(s_i)} \sum\limits_{j=1}^{M} \left\| (s_i\boldsymbol{E}(\lambda_j) - \boldsymbol{A}(\lambda_j))\boldsymbol{X}(s_i) - \boldsymbol{B}(\lambda_j) \right\|_\mathrm{F}^2 \\ \text{s.t.} \quad \boldsymbol{X}(\mathrm{s_i}) \in \mathbb{C}^{n\times 1} \end{cases} \tag{8}$$

where, $\|\cdot\|_\mathrm{F}$ represents the Frobenius norm, $\lambda_j \in \mathbb{S}$ represents the system parameters interpolation points, and M represents the number of parameter interpolation points. The optimal solution in (8) can be reformulated by the recursive least squares method as in (9).

$$\boldsymbol{X}(s_i) = \left(\sum_{j=1}^{M} \boldsymbol{M}_i(\lambda_j)^\mathrm{H} \boldsymbol{M}_i(\lambda_j) \right)^{-1} \times \sum_{j=1}^{M} \boldsymbol{M}_i(\lambda_j)^\mathrm{H} \boldsymbol{B}(\lambda_j) \tag{9}$$

where, $\boldsymbol{M}_i(\lambda_j) = s_i\boldsymbol{E}(\lambda_j) - \boldsymbol{A}(\lambda_j)$.

In the aforementioned $\boldsymbol{T}_p$ derivation process (7) and (9), the accuracy of the parametric reduced order model built by the traditional KS-PMOR method depends on both system parameters interpolation strategies and the frequency interpolation strategies. However, in the current literature, there are rare general algorithms for the optimization of the system parameters and frequency interpolation strategies. Thus, it is difficult to build the high-precision PROIMs of REMGs by directly using the traditional KS-PMOR method.

3.2 Proposed AP-IMOR Method

To overcome the aforementioned issues, the AP-IMOR method incorporating an adaptive interpolation optimization algorithm is originally proposed in this paper as a general method for forming the PROIM of REMGs. In the proposed AP-IMOR method, the adaptive interpolation optimization algorithm contains two parts: system parameters interpolation optimization and frequency interpolation optimization.

3.2.1 System Parameters Interpolation Optimization

As aforementioned, the projection matrix $\boldsymbol{T}_p$ is spanned by the $\boldsymbol{X}(s_i)$ at each frequency interpolation point. The basic requirement for solving high-accuracy $\boldsymbol{X}(s_i)$ according to (9) is that the optimal solution of $\boldsymbol{X}(s_i)$ can converge. In general, convergence of $\boldsymbol{X}(s_i)$ can be well achieved by increasing the system parameters interpolation points in $\mathbb{S}$. However, the increasing number of system parameter interpolation points will introduce additional error to $\boldsymbol{X}(s_i)$ during the iterative solving of (9), as presented in (10):

$$\begin{cases} \boldsymbol{B}_\mathrm{esum}(s_i) = \sum\limits_{j=1}^{N} \left| (s_i\boldsymbol{E}(\lambda_j) - \boldsymbol{A}(\lambda_j))\boldsymbol{X}(s_i) - \boldsymbol{B}(\lambda_j) \right| \\ \boldsymbol{X}_\mathrm{err}(\mathrm{s_i}) = \boldsymbol{B}_\mathrm{esum}(s_i) M_\mathrm{cond} \end{cases} \tag{10}$$

where, $\boldsymbol{B}_{esum}(s_i)$ is named as the cumulative error of $\boldsymbol{B}(\boldsymbol{\lambda}_j)$ in this paper. $\boldsymbol{X}_{err}(s_i)$ represents the cumulative error of $\boldsymbol{X}(s_i)$ at the frequency interpolation point s_i. It can be seen from (10) that the increasing number of system

parameters interpolation points will enlarge $\boldsymbol{B}_{esum}(s_i)$. Moreover, for practical physical systems such as REMGs with a larger condition number M_{cond} ($M_{cond} \gg 1$) of $\boldsymbol{M}_i(\boldsymbol{\lambda}_j)$, a smaller $\boldsymbol{B}_{esum}(s_i)$ may lead to a larger cumulative error $\boldsymbol{X}_{err}(s_i)$ [11]. This can enlarge the side effect of $\boldsymbol{B}_{esum}(s_i)$ on the accuracy of the obtained parametric reduced order model.

In addition, during the solving of $\boldsymbol{X}(s_i)$, the accuracy of the obtained $\boldsymbol{X}(s_i)$ is also impacted by the convergence of the optimizations. In this paper, $\boldsymbol{E}_c(s_i)$ is defined as the convergence error of $\boldsymbol{X}(s_i)$, as in (11).

$$\boldsymbol{E}_c(s_i) = \left| \boldsymbol{X}_N(s_i) - \boldsymbol{X}_{N\text{-}1}(s_i) \right| \tag{11}$$

where $\boldsymbol{X}_N(s_i)$ and $\boldsymbol{X}_{N\text{-}1}(s_i)$ represent the $\boldsymbol{X}(s_i)$ obtained in the N^{th} and $(N\text{-}1)^{\text{th}}$ iteration, $|\cdot|$ denotes the mod operation of each element in the matrix. For the state vector $\boldsymbol{X}(s_i)$ with large variations in $\mathbb{S}$, a larger number of parameter interpolation points are needed to ensure the convergence of $\boldsymbol{X}(s_i)$. However, more parameter interpolation points will introduce larger cumulative errors to $\boldsymbol{X}(s_i)$ as in (10).

According to the above discussions, the effect of the system parameters interpolation strategy on the accuracy of the PROIM can be further localized to the convergence error and cumulative error of $\boldsymbol{X}(s_i)$. Thus, the optimization of system parameters interpolation should take the constraints of convergence error and cumulative error at the same time. The formulation of system interpolation optimization is shown in (12):

$$\begin{cases} \min\limits_{\boldsymbol{X}_k(s_i)} \sum\limits_{j=1}^{N} \left\| (s_i \boldsymbol{E}(\lambda_j) - \boldsymbol{A}(\lambda_j)) \boldsymbol{X}_k(s_i) - \boldsymbol{B}(\lambda_j) \right\|_{\text{F}}^2 \\ \text{s.t.} \quad \boldsymbol{X}_k(s_i) \in \text{C}^{n\times 1} \qquad 1 \le k \le k_{ps} \\ \quad \max(\boldsymbol{E}_C(s_i)) \le \text{Th}_{conv} \\ \quad \max(\boldsymbol{X}_{err}(s_i)) < \text{Th}_{err} \end{cases} \tag{12}$$

where $\boldsymbol{X}_k(s_i)$ is the state vector obtained at the frequency interpolation point s_i in the k^{th} parameter subspace, $\max(\cdot)$ represents the operation of obtaining the maximum elements in the matrix. During solving (12), the parameter interpolation strategy (including N and k_{ps}) are tuned so that the solving process for $\boldsymbol{X}_k(s_i)$ can meet the error constraints.

3.2.2 Frequency Interpolation Optimization

In the traditional KS-PMOR method, the projection matrix $\boldsymbol{T}_p$ should be able to access all regions in the state space of the original full-order model so that all states of the original full-order model can be projected to a smaller state space to ensure the accuracy of the obtained PROIM [12]. To quantify the region accessing of state space for the original full-order model, the following ***Lemma*** is introduced.

Lemma: In the state space $\mathbb{V}$, if all regions in $\mathbb{V}$ can be accessed by the vectors group $\boldsymbol{J}$, the $\boldsymbol{J}$ rank is equal to the number of basis vectors in $\mathbb{V}$.

Proof: If all regions in the state space $\mathbb{V}$ can be accessed by vectors group $\boldsymbol{J}$, it means that any vector $\boldsymbol{\beta}$ in $\mathbb{V}$ can be represented by $\boldsymbol{J}$. That is, the d linearly independent vectors $\boldsymbol{J}_b=\{\boldsymbol{J}_1, \boldsymbol{J}_2, \ldots, \boldsymbol{J}_d\}$ in $\boldsymbol{J}$ form a group of basis vectors of $\mathbb{V}$, and the remaining vectors in $\boldsymbol{J}$ can also be linearly represented by $\boldsymbol{J}_b$, then $\boldsymbol{J}_b$ is a maximal linearly independent group of $\boldsymbol{J}$, and $rank(\boldsymbol{J})=d$ can be obtained.

Consequently, to construct a high-rank projection matrix, some important frequency interpolation points should be included during the projection derivation. In this section, the rank-sensitive sub-frequency bands are first acquired by the frequency window scanning, as shown in Fig. 2. Thereafter, the frequency interpolation points in the rank-sensitive sub-frequency bands are added to include the important frequency interpolation points according to (13).

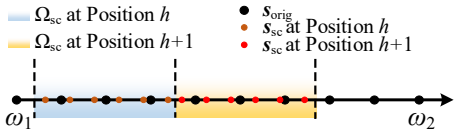

Fig. 2. Diagram of frequency window scanning.

During the frequency window scanning, the frequency window Ω_{sc} is established, and the reduced order frequency band $\Omega=[\omega_1, \omega_2]$ is scanned by the Ω_{sc} from the ω_1 to ω_2, as in Fig. 2, where, s_{orig} is the original frequency interpolation points in Ω. For each position of the frequency window, the s_{orig} in the frequency window is replaced by the s_{sc}, and the rank sensitivity L_r is calculated by $L_{r,h} = \partial R_{T,h} / \partial g \quad (L_h \ge 0)$. $L_{r,h}$ and $R_{T,h}$ represent the rank sensitivity and the rank of the projection matrix when the frequency window is at the h-th position, respectively. According to the rank sensitivity L_r, the rank-sensitive sub-frequency bands Ω_{sub} can be obtained.

To maximize the rank of $\boldsymbol{T}_p$, the number of frequency interpolation points in the obtained rank-sensitive sub-frequency bands Ω_{sub} is optimized by (13).

$$\begin{cases} \max\ rank(\boldsymbol{T}_p) = rank(\text{span}\{\boldsymbol{X}(\boldsymbol{s}_{sub}), \boldsymbol{X}(\boldsymbol{s}_{res})\}) \\ \text{s.t.} \quad Q = \min(\boldsymbol{Q}_T) \\ \quad \boldsymbol{s}_{sub} \in \Omega_{sub}, \boldsymbol{s}_{res} \in \Omega_{res} \end{cases} \tag{13}$$

where, Ω_{res} is the rank-insensitive sub-frequency bands. $\boldsymbol{s}_{sub}$ and $\boldsymbol{s}_{res}$ are the sets of the frequency interpolation points in Ω_{sub} and Ω_{res}, respectively. $\boldsymbol{Q}_T$ is the set of frequency interpolation points number that can maximize the rank of $\boldsymbol{T}_p$. Q is chosen as the minimum value in $\boldsymbol{Q}_T$ to prevent introducing additional errors in $\boldsymbol{T}_p$.

Based on the aforementioned system parameter and frequency interpolation strategies, the proposed AP-IMOR method can be formed into four stages, its framework is represented in Fig. 3:

Stage 1. Optimizing parameters interpolation

strategy: In this stage, cumulative errors and the convergence errors of $\boldsymbol{X}(s_i)$ are introduced as the constraints to reform the optimizing problem in (12). The obtained optimized parameter interpolation strategy can converge $\boldsymbol{X}(s_i)$ without excessive cumulative errors.

Stage 2. Optimizing frequency interpolation strategy: The second stage is followed after the parameter interpolation optimization. In this stage, the rank maximization of the projection matrix is set as the objective function, and this objective is achieved by adjusting the number of frequency interpolation points in the rank-sensitive sub-frequency band.

Stage 3. Projection matrices construction: Based on the obtained parameter interpolation strategy and the frequency interpolation strategy, the projection matrix $\boldsymbol{T}_p$ can be easily derived according to the equation (7) and (9).

Stage 4. Building the PROIMs of REMGs: the full-order model of REMG can be projected to a small state space by the obtained $\boldsymbol{T}_p$ according to (5), and the PROIM of REMG can be derived by (3).

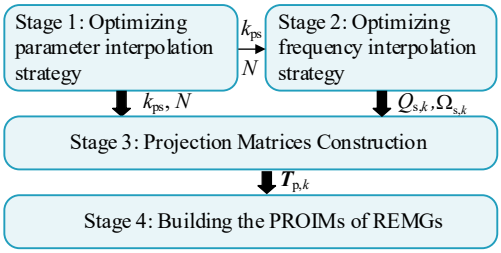

Fig. 3. Framework of proposed AP-IMOR method.

4 Simulation Verification and Discussions

In this paper, the proposed method is evaluated based on two different scales of REMGs. The accuracy of the proposed method is evaluated based on a small-scale REMG with 4 paralleled CREGs. To further verify the effectiveness of the proposed method on the actual oscillatory analysis, the PROIM of a large-scale REMG containing 18 different CREGs is established and tested under the RTDS platform.

4.1 REMG with Four Paralleled CREGs

In this section, a small-scale REMG with four paralleled CREGs is used to evaluate the accuracy of the proposed method. The detailed parameters of four paralleled CREGs are shown in Table 1. The PROIM of the small-scale REMG is built by the proposed method and compared with three other different methods listed in Table 2. The output current I_{d0} of REMG at steady state setpoints is taken as a preserved parameter during the model order reduction.

Among these three methods, Method 1 is the traditional KS-PMOR without interpolation optimizing, Method 2 and Method 3 can meet part of the error constraints. The accuracy of the PROIM in the first parameter subspace built by different methods is compared to verify that the proposed method can improve the error performance of the obtained PROIM, as in Fig. 4.

Table 1. Detailed Parameters of REMG with Four Paralleled CREG

Parameter Value	Value and Variation	Parameter Value	Value and Variation
Rated power	660kW	K_c	0.75 (±33% Random)
L_m (μH)	405 (±4% Random)	K_{ppll}	625 (±12% Random)
C (μF)	145 (±7% Random)	K_{ipll}	8000
L_g (μH)	8 (±12.5% Random)	ω_p (rad/s)	637.5 (±6% Random)
R_c (mΩ)	28.5 (±12.5% Random)	I_{d0} (A)	1420
K_{ip}	1.55 (±42% Random)	U_{pcc0} (V)	311
K_{ii}	35	f_s (kHz)	10

Table 2. Satisfaction of Constraints by Different Interpolation Strategies

Method	Convergence Error Constraint	Cumulative Error Constraint	$\boldsymbol{T}_p$ Rank Maximum
Method 1	×	×	×
Method 2	√	×	×
Method 3	√	√	×
FDA-PMOR	√	√	√

The magnitude and phase errors of the PROIM built based on different interpolation strategies are presented in Fig. 4. The model order reduction errors are mostly concentrated in the low-frequency band where the frequency characteristics are dominated by I_{d0}. The maximum magnitude and phase error of the PROIM in the proposed method can be reduced to 0.4 dB and 1.0°, respectively. Compared with methods 1-3, the maximum magnitude error with Strategy 4 is reduced by 93.15%, 75.7%, and 74.34%, respectively; and the maximum phase errors are reduced by 81.4%, 60.42%, and 60.66%, respectively. According to the above comparisons, it can be seen that the proposed method can significantly improve the error performance of the PROIM.

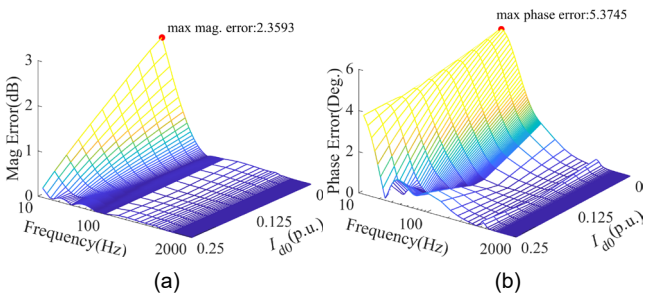

(a) (b)

 DOI:10.30420/566414095

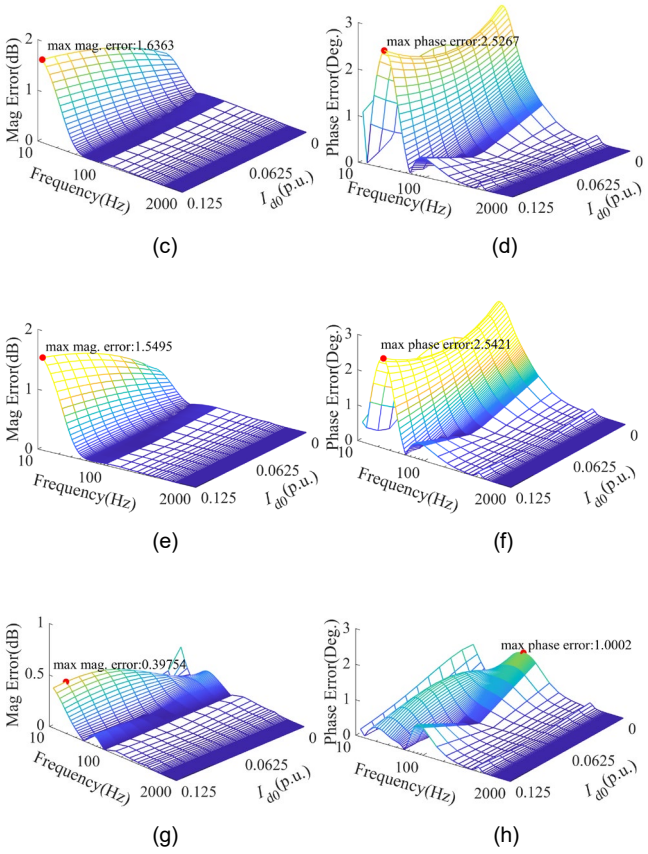

Fig. 4. Model order reduction errors vs. I_{d0} and frequency. Magnitude errors are shown in the left column for (a) Method 1, (c) Method 2, (e) Method 3, and (g) Method 4; phase errors are shown in the right column for (b) Method 1, (d) Method 2, (f) Method 3, and (h) Method 4.

4.2 Large-Scale REMG with 18 Paralleled CREGs

The actual REMGs usually consist of a large number of CREGs with different parameters and rated power. In this section, the PROIM of a 4.2 MW large-scale REMG is built by the proposed method. The specific parameters of each CREG are presented in Table 3.

4.2.1 Error Evaluation of the Obtained PROIM

The PROIM of large-scale REMG can be built according to the proposed AP-IMOR. The output current I_{d0} of REMG at steady state setpoints is taken as the preserved parameter. By the proposed method, the parameter space of I_{d0} is segmented into 10 parameter subspaces. The magnitude and phase errors of the obtained PROIM have also been presented in Fig. 5.

From Fig.5, it can be observed that most of the magnitude and phase errors can be maintained within 0.5 dB and 1 degree, respectively. Moreover, with the proposed method, the model size of each local PROIM can be controlled around 23 orders, which is 82% less than the 126-order full-order impedance model. Compared with the small-scale REMG with four paralleled CREGs, the model size of the large-scale REMG can be reduced more notably by the proposed method. Thus, the proposed method has better suitability for model order reduction of large-scale REMG.

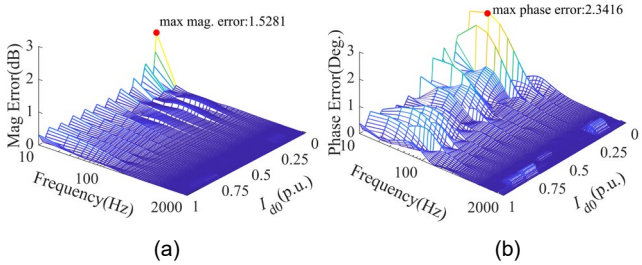

Fig. 5. Model order reduction errors vs. I_{d0} and frequency: (a) magnitude errors, and (b) phase errors.

Table 3. Detailed Parameter of 4.2MW Large-scale REMG

Parameter	Value and Variation	Parameter	Value and Variation
Type A Inverter*6			
Rated Power	100kW	K_c	2.25 (±11% Random)
L_m (μH)	625 (±12% Random)	K_{pllp}	2250 (±11% Random)
C (μF)	62.5 (±20% Random)	K_{plli}	8000
L_g (μH)	62.5 (±12% Random)	ω_p (rad/s)	1250 (±20% Random)
R_c (mΩ)	125 (±20% Random)	I_{dN} (A)	215
K_{ip}	2.25 (±11% Random)	U_N (V)	311
K_{ii}	100	f_s (kHz)	10
Type B Inverter*6			
Rated Power	250kW	K_c	1.75 (±14.3% Random)
L_m (μH)	250 (±20% Random)	K_{pllp}	2150 (±11.6% Random)
C (μF)	187 (±26.7% Random)	K_{plli}	8000
L_g (μH)	8.1 (±30.9% Random)	ω_p (rad/s)	1050 (±23.8% Random)
R_c (mΩ)	125 (±20% Random)	I_{dN} (A)	537.5
K_{ip}	2.25 (±11% Random)	U_N (V)	311
K_{ii}	125	f_s (kHz)	10
Type C Inverter*6			
Rated Power	350kW	K_c	0.75 (±33% Random)
L_m (μH)	68 (±14.7% Random)	K_{pllp}	1850 (±13.5% Random)
C (μF)	270 (±18.5% Random)	K_{plli}	8000
L_g (μH)	15 (±33% Random)	ω_p (rad/s)	1750 (±14.3% Random)
R_c (mΩ)	95 (±26.3% Random)	I_{dN} (A)	751
K_{ip}	0.75 (±33% Random)	U_N (V)	311
K_{ii}	150	f_s (kHz)	10
Grid Parameters			
SCR	0.92	R_{rec} (Ω)	0.01
C_{rec} (mF)	13.5		

4.2.2 Application of the obtained PROIM to the Oscillatory Stability Analysis

The real-time simulation platform for the large-scale REMG is established based on the RTDS simulator as shown in Fig. 6. The detailed parameters of the external grid can be found in Table 3.

The oscillatory stability analysis of the grid-tied larger-scale REMG is evaluated by the obtained PROIM. To simulate the varying operating points of the actual REMG, the normalized output power data from a practical photovoltaic generator-based REMG is fed into the obtained PROIM as I_{d0}. The output power data set contains one-day data with a resolution of 5 min (288 data points included).

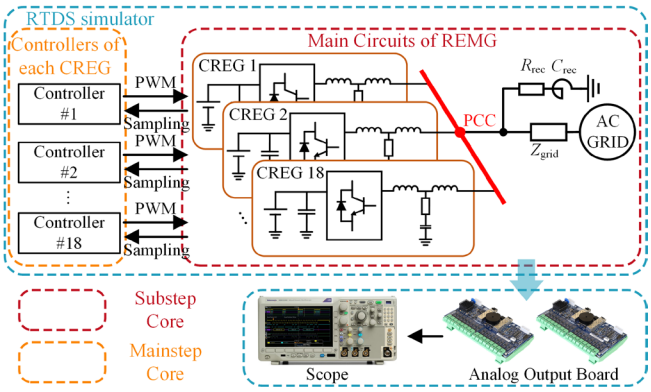

Fig. 6. Real-time simulation platform of large-scale REMG based on RTDS.

The comparison of the computational burden in the process of SSSA by the full-order IM and the PROIM is shown in Table 4.

It can be seen that, by replacing the full-order IM with the obtained PROIM, the time consumption of the SSSA can be reduced by 77.5%, meanwhile, the memory usage can be decreased by 97.6%. Therefore, the PROIM can significantly reduce the computational burden during the SSSA of the investigated REMG.

Table 4. Computational Burden Comparison

	Time Consumption	Memory Usage
Full Order IM	49.195s	25972KB
PROIM	11.068s	616KB

The error distribution of the stability phase margin obtained based on the PROIM is shown in Fig. 7. It can be seen that most of the phase margin errors are located in ±2%.

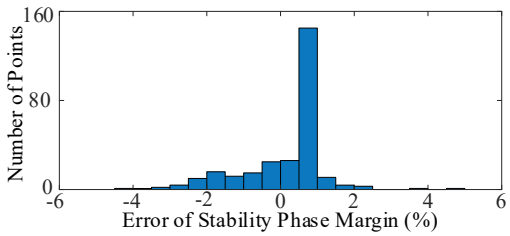

Fig. 7. Error distribution of stability phase margin.

According to the simulation in this section, for the REMGs at a large scale, the computational efficiency of SSSA can be improved by replacing the full-order IM with the obtained PROIM, and the stability phase margin obtained by the obtained PROIM has a superior error performance. Consequently, the PROIM built by the proposed AP-IMOR method is promising for the seconds-level and minutes-level online oscillatory stability analysis of power systems with clusters of REMGs.

Additionally, the critical instability case that occurs with the power fluctuation of the REMG is presented and analyzed separately. In this case, the output power of REMG increases from 0.67 p.u. to 0.77 p.u.. The oscillatory stability is assessed by the impedance return ratio L in (14).

$$L(s) = Z_{eg}(s) / Z_{MCFS}(s) \tag{14}$$

where $Z_{MCFS}(s)$ and $Z_{eg}(s)$ represent the equivalent impedance of large-scale REMG and the external grid at PCC, respectively.

During the oscillatory stability analysis, the full-order impedance model and the different PROIMs of REMG are substituted into (14). The Nyquist diagrams with different output power are shown in Fig. 8, where L_f, $L_{KS\text{-}PMOR}$, and $L_{AP\text{-}IMOR}$ represent the impedance return ratios based on the full-order impedance model, traditional KS-PMOR, and the proposed AP-IMOR, respectively.

In Fig. 8, the Nyquist curves of $L_{FDA\text{-}PMOR}$ and L_f are well consistent with each other. The Nyquist curve encircles the point (-1,0) when the output power of the REMG increases, which means the system enters the unstable region. From the interaction point of the Nyquist curve and the unit circle, the theoretically unstable oscillation frequencies using L_f and $L_{AP\text{-}IMOR}$ are 26.5 Hz and 26 Hz in the dq-domain. However, the Nyquist curves of $L_{KS\text{-}PMOR}$ are mismatched with the L_f.

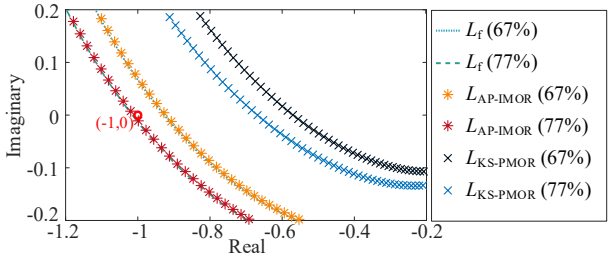

Fig. 8. Nyquist diagram of $L(s)$ during output power changing.

The time-domain experimental results based on the real-time simulation platform are presented in Fig. 9. It can be found that the active output power P and the three-phase output current $I_{a,b,c}$ measured at the PCC point of the REMG suffer sub-synchronous oscillations after the power increasing. The FFT analysis of I_a shows that the oscillation frequencies are 23 Hz and 77 Hz, corresponding to 27 Hz in the dq-domain. This result is consistent with the theoretical analysis by L_f and

$L_{\text{AP-IMOR}}$, but the $L_{\text{KS-PMOR}}$ incorrectly evaluates the stability boundary.

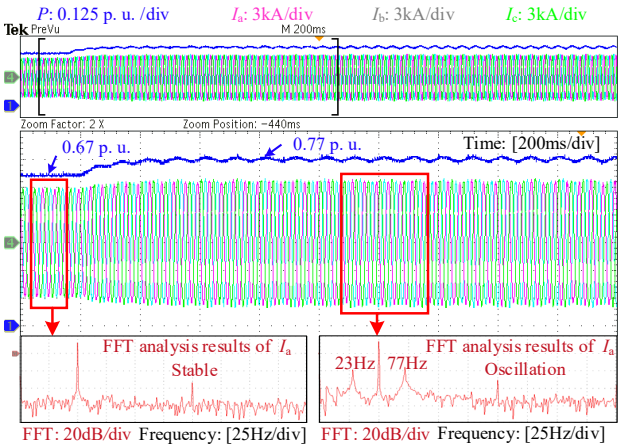

Fig. 9. Real-time simulation results of power fluctuation.

According to the above analysis, the effectiveness of the PROIM built by the proposed AP-IMOR method for actual oscillatory stability analysis has been verified.

5 Conclusions

In this paper, the AP-IMOR method with an adaptive interpolation optimization algorithm is originally proposed as a general method to obtain the high-precision PROIM of REMGs. Comparing the other three methods without full optimization of the interpolation strategy, the proposed method reduces the magnitude and phase error of the obtained PROIM by up to 93.15% and 81.4%, respectively. For the large-scale REMGs, the model size of the obtained PROIM is only 18.3% of the full-order model with a high model accuracy.

Furthermore, the obtained PROIMs of the large-scale REMGs have been applied to the SSSA in this paper. Compared with the full-order IM, the computation time and memory usage of the SSSA based on the obtained PROIM can be reduced by about 77.5% and 97.6%, respectively. Besides, the stability phase margin error of SSSA obtained from the obtained PROIM can be controlled within ±5%. This means that the PROIM obtained by the proposed method is promising for the seconds-level and minutes-level online SSSA in regional power systems with several large-scale MCFSs. It is worth mentioning that the proposed method can realize the model order reduction without simplifying any specific links in the original full-order impedance model of the REMG. Thus, the proposed method is general and can apply to the PROIM of different REMGs such as distributed renewable energy power stations, wind farms, and alike.

In our future work, more detailed validation cases will be supplemented to comprehensively evaluate the proposed method.

6 Acknowledgment

This work was supported by Open Fund of State Key Laboratory of Operation and Control of Renewable Energy & Storage Systems (China Electric Power Research Institute) [No. NYB51202201695], National Natural Science Foundation of China under Grant [No. 51677050] and 111 Project [No. BP0719039].

7 References

[1] E Bullich-Massagué, F Díaz-González, M Aragüés-Peñalba, Girbau-Llistuella, F. , Olivella-Rosell, P. , Sumper, A. , "Microgrid clustering architectures," in Applied Energy, vol. 212, no. 15, pp. 340-361, Feb. 2018.

[2] Jeff Billo, et al, "Inaugural Research Agenda," Global Power System Transformation (G-PST) Consortium, Colombia, SC, Tech. Rep, 2022.

[3] J. Sun, "Two-Port Characterization and Transfer Immittances of AC-DC Converters–Part II: Applications," in IEEE Open Journal of Power Electronics, vol. 2, pp. 483-510, 2021.

[4] S. Kamala, N. B. Y. Gorla and S. K. Panda, "Small-Signal Stability Improvement of Microgrid With Battery Energy Storage System Based on Real-Time Grid Impedance Measurement," in IEEE Transactions on Industry Applications, vol. 58, no. 2, pp. 2537-2546, March-April 2022.

[5] W. Du, B. Ren, H. Wang and Y. Wang, "Comparison of Methods to Examine Sub-Synchronous Oscillations Caused by Grid-Connected Wind Turbine Generators," in IEEE Transactions on Power Systems, vol. 34, no. 6, pp. 4931-4943, Nov. 2019.

[6] H. Liu, X. Xie, X. Gao, H. Liu and Y. Li, "Stability Analysis of SSR in Multiple Wind Farms Connected to Series-Compensated Systems Using Impedance Network Model," in IEEE Transactions on Power Systems, vol. 33, no. 3, pp. 3118-3128, May 2018.

[7] H. R. Ali, L. P. Kunjumuhammed, B. C. Pal, A. G. Adamczyk and K. Vershinin, "Model Order Reduction of Wind Farms: Linear Approach," in IEEE Transactions on Sustainable Energy, vol. 10, no. 3, pp. 1194-1205, July 2019.

[8] Z. Zhang, I. M. Elfadel and L. Daniel, "Model order reduction of fully parameterized systems by recursive least square optimization," 2011 IEEE/ACM International Conference on Computer-Aided Design (ICCAD), 2011, pp. 523-530.

[9] Benner, Peter, G. Serkan and W. Karen. "A survey of projection-based model reduction methods for parametric dynamical systems." in SIAM review, vol. 57, no. 4, pp. 483-531, November 2015.

[10] D. Zhu, S. Zhou, X. Zou and Y. Kang, "Improved Design of PLL Controller for LCL-Type Grid-Connected Converter in Weak Grid," in IEEE Transactions on Power Electronics, vol. 35, no. 5, pp. 4715-4727, May 2020.

[11] Golub, Gene H., and Charles F. Van Loan. Matrix computations. JHU Press, 2013.

[12] B. N. Bond and L. Daniel, "A Piecewise-Linear Moment-Matching Approach to Parameterized Model-Order Reduction for Highly Nonlinear Systems," in IEEE Transactions on Computer-Aided Design of Integrated Circuits and Systems, vol. 26, no. 12, pp. 2116-2129, Dec. 2007.